Leaky-Wave Radiation From 2-D Dielectric Lattices Excited by an Embedded Electric Line Source

Paolo Baccarelli, *Member, IEEE*, Ludovica Tognolatti, *Graduate Student Member, IEEE*, Vakhtang Jandieri, *Senior Member, IEEE*, Silvio Ceccuzzi, Cristina Ponti, *Member, IEEE*, and Giuseppe Schettini, *Senior Member, IEEE*

***Abstract*— This article presents an analytical and numerical investigation of the radiation features of an interesting class of electromagnetic bandgap (EBG) structures excited by an electric line source. The radiation from 2-D lattices made with lossless dielectric cylinders, typically optimized by using the Bloch analysis of the corresponding 2-D photonic crystals, is originally investigated in terms of leaky waves. A thorough modal analysis of open waveguides, composed of a finite number of periodic chains of circular dielectric rods, is presented, which shows a multiplicity of bound and leaky modes. Two radiation windows are identified and the relevant directive features are described in terms of properly excited dominant leaky modes. The possible excitation of higher order leaky modes and guided modes has been carefully considered, by also capturing the relevant residue contributions in a nonspectral representation of the excited fields. The final results on radiated fields by realistic truncated structures, obtained by *ad hoc* software as well as full-wave EM simulators, are in excellent agreement with those predicted by the proposed leaky-wave approach.**

***Index Terms*— Directive radiation, electromagnetic bandgap (EBG) antennas, leaky waves, leaky-wave antennas (LWAs), periodic structures.**

I. Introduction

PHOTONIC crystals have been widely studied in recent decades. Electromagnetic bandgap (EBG) materials are composite *periodic* structures, with similar characteristics to photonic crystals in the microwave field. They can be classified as homogenizable structures, which operate at wavelengths much larger than the lattice period [1]–[3], or as standard lattices exploiting the periodicity at wavelengths comparable to the lattice period [4], [5]. As concerns the latter, several works have been carried out to demonstrate how such EBG materials can improve the performance of antennas [6]. Depending on the EBG structure used, two different radiation mechanisms can be identified [7]. EBG operating in the stopband region is used to build the Fabry–Perot cavity antennas with high directivity [8]–[13]. EBG lattice structures operating outside the stopband allow for solutions of the wave equation in the form of Bloch waves [4], [5]. In all cases, high values of the directivity are shown, e.g., as summarized in [7], which are comparable with those obtainable with different approaches, e.g., by using printed metasurfaces as in [14]–[16], whereas EBG dielectric lattices can be preferred at those frequencies where ohmic losses become challenging [17]. Furthermore, in EBG lattices, it is possible to explore peculiar radiative performances of a primary source [18], which are alternative to those observed in conventional cavity antennas exploiting the bandgap region.

The band diagrams of the Bloch waves propagating in the 2-D photonic crystal shown in Fig. 1(a) represent an important tool to grasp the physical behavior and perform a preliminary design of EBG antennas based on lattice of circular dielectric rods [5], [19]. Despite its usefulness, such an approach only gives very qualitative information about the radiation pattern of a real antenna, which is truncated in both dimensions, as shown in the sketch of Fig. 1(c). To accurately predict such radiative features, full-wave (mostly numerical) approaches, such as time- and frequency-domain and/or boundary integral equation methods, are generally employed [20], [21], but they partially hide the true physical mechanism, which is behind the obtained results. It follows that the gap between the first and the second design steps, respectively, based on band diagrams and full-wave solvers, is large and the optimization phase of a realistic 3-D antenna is time-consuming.

An alternative procedure is proposed here, which considers the dielectric EBG lattice antennas in Fig. 1(c) as open waveguides composed by a stack (along a transverse direction) of infinite periodic chains, as shown in Fig. 1(b). The advantage of the considered approach is that the radiative features of the EBG antenna can be rigorously described in terms of the leaky modes [22], [23] propagating along the open waveguide. Such perspective is of great aid to both antenna

Manuscript received January 18, 2021; revised April 15, 2021; accepted April 24, 2021. Date of publication June 2, 2021; date of current version October 28, 2021. This work was supported in part by the Italian Ministry for Education, University, and Research through the Project PRIN 2017 (WPT4WID: Wireless Power Transfer for Wearable and Implantable Devices) under Grant 2017YJE9XK_005 and in part by the Shota Rustaveli National Science Foundation of Georgia (SRNSFG) under Grant FR-19-4058. *(Corresponding author: Paolo Baccarelli.)*

Paolo Baccarelli, Ludovica Tognolatti, Cristina Ponti, and Giuseppe Schettini are with the Department of Engineering, Roma Tre University, 00146 Rome, Italy, and also with CNIT, Roma Tre University, 00146 Rome, Italy (e-mail: paolo.baccarelli/ludovica.tognolatti/etc@uniroma3.it).

Vakhtang Jandieri is with the Department of General and Theoretical Electrical Engineering (ATE), Faculty of Engineering, University of Duisburg–Essen and Center for Nanointegration Duisburg-Essen (CENIDE), D-47048 Duisburg, Germany (e-mail: vakhtang.jandieri@uni-due.de).

Silvio Ceccuzzi is with the Department of Engineering, Roma Tre University, 00146 Rome, Italy, and also with the Fusion and Nuclear Safety Department, Italian Energy and Environment Agency (ENEA), 00044 Frascati, Italy (e-mail: silvio.ceccuzzi@enea.it).

Color versions of one or more figures in this article are available at https://doi.org/10.1109/TAP.2021.3083768.

Digital Object Identifier 10.1109/TAP.2021.3083768

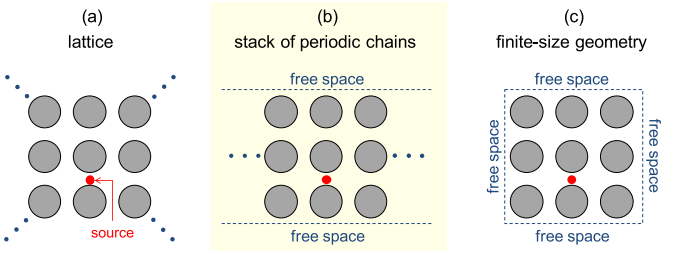

Fig. 1. EM problem of an EBG structure with an embedded source approached in terms of (a) Bloch, (b) leaky, and (c) scattered waves.

design and physical understanding because it takes advantage of the powerful tools provided by the well-grounded theory of leaky-wave antennas (LWAs) [24], [25], which is based on the knowledge of the leaky-mode complex wavenumbers. This procedure can be thought at an intermediate step in the antenna design flow, as shown in the sketch of Fig. 1.

In this article, the radiation mechanism of 2-D periodic dielectric lattices proposed by Enoch *et al.* [4], [5] is thoroughly examined in terms of leaky waves. In a similar framework, previous studies were proposed for artificial material slabs made by periodic conducting cylinders [26], by homogenizable and metallic photonic crystals [27]–[30], typically known as wire medium slabs, and by photonic dielectric quasicrystals (i.e., nonperiodic crystals) [31], [32], whereas modal evolutions and coupling phenomena in arrays of metallic cylinders embedded in a grounded dielectric slab were investigated in [33]. In the different areas of interest of the interaction between light and photonic crystal slabs, resonances of reflection and transmission spectra have been related to the existence of leaky modes. In particular, measured and simulated transmission curves have been converted into approximated band diagrams, where, however, only the phase constants of the involved leaky modes were reported [34], [35]. In all cases, a deep investigation of the modal spectrum supported by the EBG *dielectric* lattices, in periodic and nonhomogenizable configurations, and of the dispersion behavior of the relevant leaky *complex* wavenumbers, i.e., of both the phase and the attenuation constants, to be used in quantitative design rules, was not provided. A brief preliminary overview is presented in [36]. Here, a complete numerical and analytical study is reported by providing all the details and reporting a comprehensive set of results and validations with the relevant thorough discussion.

In particular, an extensive full-wave modal analysis of bound and leaky modes supported by a finite number of periodic chains of dielectric circular rods of infinite length is first performed, which extends the study reported in [37] where only a single periodic chain was considered. The highly multimodal nature of the EBG open waveguide is carefully investigated and different radiative frequency regions are described in terms of physical leaky modes supported by the structure. These achievements confirm that directive radiation can be suitably obtained in EBG lattice antennas, as predicted by the canonical analysis based on the Bloch modes of the 2-D infinite crystal, and provide much physical insight.

The considered EBG open waveguide is then excited by an electric line source and the relevant radiation features are investigated. Due to the multimodal nature of the EBG structure, an accurate analysis of the modal fields and the interaction between fields and source is performed in order to define the positions for the line source that allow for the desired radiative features (e.g., highly efficient directive radiation at broadside). The contribution to the radiated field of the excited leaky modes is rigorously considered by considering the relevant residue contributions in a spectral-domain representation of the antenna aperture fields [38]–[40]. The possibility of exciting poorly attenuated leaky modes in the absence of any other bound mode is explored, with the aim at designing efficient directive truncated radiators with limited edge diffraction, and simple design formulas are used to optimize the radiators [24], [25].

Here, different analytical and numerical approaches are applied for the accurate investigation and design of this class of structures. Band diagrams of the Bloch modes of 2-D infinite crystals are derived with an in-house code based on the plane-wave expansion (PWE) method [41]. Leaky-mode complex wavenumbers are obtained by using an *ad hoc*, rigorous, agile, and efficient formulation based on the lattice sums (LSs) technique by means of the Ewald approach [37], [42]. The far field radiated by an elementary line source embedded in the infinite EBG lattice waveguides is derived by using a suitable spectral-domain method [43], which also allows for rigorously accounting for the residue contributions of the excited leaky modes of the open waveguide. Fields radiated by an electric line source embedded in truncated EBG lattice structures are obtained by using an *ad hoc* cylindrical wave approach (CWA) [44]. Validation of the results obtained for the infinite and truncated structures excited by an electric line source has been performed by using a full-wave EM commercial software, i.e., CST Microwave Studio [45].

This article is organized as follows. Section II gives the main theoretical background about the design approach based on the dispersion-band diagrams for the infinite 2-D photonic crystal, whereas Section III presents a detailed analysis of bound and leaky modes propagating along a stack of periodic chains of circular cylinders. The Brillouin dispersion diagram of the considered infinite open EBG waveguide is described, showing radiative regions and multiple leaky and guided mode propagation and describing the relevant modal field configurations. In Section IV, accurate derivations of the far fields radiated by a line source embedded in the EBG lattice waveguide are provided, for infinite and truncated structures, and the results obtained through the full-wave simulations with CST, the LSs technique, and the CWA are presented.

II. Design Approach Based on the Dispersion/Band Diagrams for the Infinite 2-D Periodic Lattice

We consider an infinite number of dielectric cylinders with circular cross section, radius r, and infinite length, aligned with the z-axis and arranged in a square lattice of period p over the xy plane in the free space. A Bloch-wave analysis is here performed for the case of the electric field aligned with

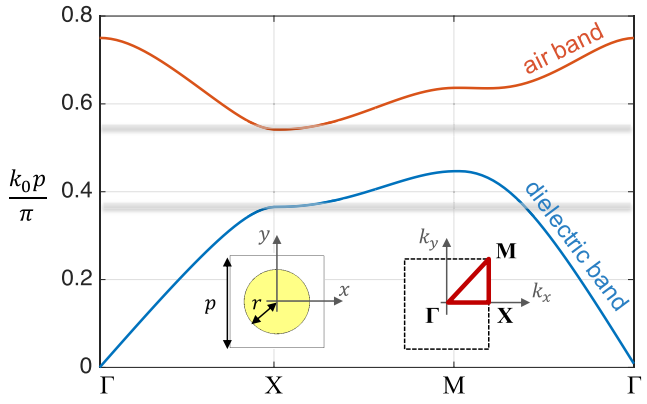

Fig. 2. Band diagram along the edge of the irreducible Brillouin zone for a square lattice of cylinders with $r = 0.35p$ and relative dielectric constant $\epsilon_r = 11.7$.

the cylinder axis z, which corresponds to TE Bloch modes with respect to the x- and y-directions. A time-harmonic dependence $e^{j\omega t}$ is assumed and suppressed throughout this article.

By applying the PWE method to the master equation of the periodic structure [41], whose square unit cell is described in the inset of Fig. 2, the following eigenvalue equation is obtained for the electric field:

$$\sum_{m,n} \kappa_{i-m,j-n} |\mathbf{G}_{m,n} + \mathbf{k}|^2 f_{m,n} = k_0^2 f_{i,j} \tag{1}$$

where

$$\mathbf{G}_{m,n} = \frac{2\pi m}{p}\hat{\mathbf{x}} + \frac{2\pi n}{p}\hat{\mathbf{y}}$$

$\mathbf{k}$ is the in-plane wavevector, $k_0 = \omega/c$ is the free-space wavenumber, and $\kappa_{m,n}$ are the Fourier coefficients of $1/\epsilon_r(x, y)$, with ϵ_r the periodic relative permittivity. The eigenfunctions $f_{m,n}$ are the Fourier coefficients of the Bloch expansion of the electric field E_z so that

$$E_z(x, y) = \sum_{m,n} f_{m,n} e^{-j(\mathbf{G}_{m,n}+\mathbf{k})\cdot(x\hat{\mathbf{x}}+y\hat{\mathbf{y}})}. \tag{2}$$

The solutions of (1) along the edge of the first irreducible Brillouin zone are shown in Fig. 2, where the normalized frequency is plotted as a function of the wavevector for a lattice of dielectric cylinders with relative dielectric constant $\epsilon_r = 11.7$ and $r/p = 0.35$. Two propagation bands, namely dielectric and air bands, are depicted by blue and red lines, respectively, while the complete bandgap region extends from $k_0 p/\pi = 0.447$ to $k_0 p/\pi = 0.542$.

By properly tuning lattice parameters, the radiation of a source embedded in the lattice can be focused along specific directions, and a directive antenna exploiting this mechanism can be conceived. Before running time-consuming, 3-D full-wave simulations, a quick, preliminary design of a suitable lattice for such EBG antennas is generally done by means of band diagrams such as the one of Fig. 2. If a monochromatic source is embedded in the lattice, the Bloch modes that can exist are given by the intersection of the lattice bands with a horizontal plane at the source frequency. When this intersection occurs just above the bandgap, i.e., where the upper

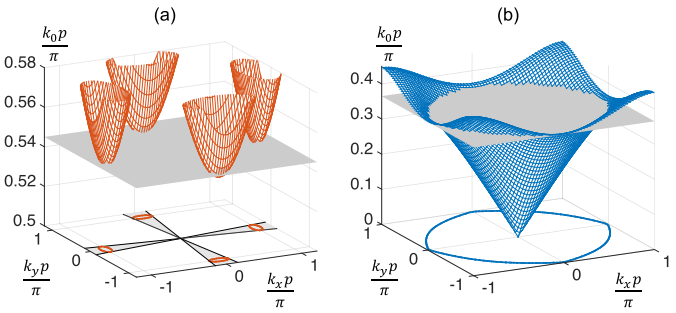

Fig. 3. Intersections of (a) air and (b) dielectric bands with horizontal planes at $k_0 p/\pi = 0.545$ and 0.365, respectively. At the bottom of the plots, the constant frequency dispersion diagrams are projected.

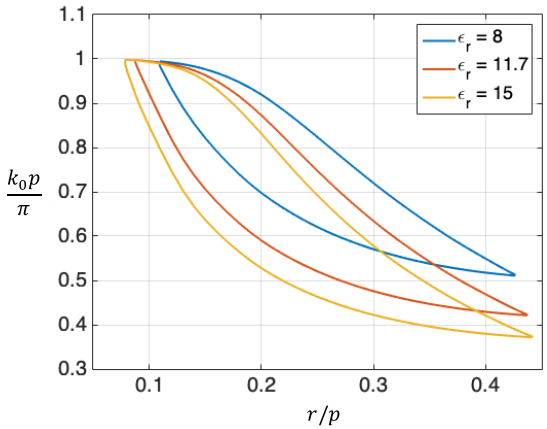

Fig. 4. Normalized frequencies at the bottom of the air band and at the top of the dielectric band versus r/p in the presence of a bandgap for three square lattices with different relative dielectric constants.

gray line of Fig. 2 encounters the lowest edge of the air band, Bloch waves propagating along either y ($k_x = 0$) or x ($k_y = 0$) are only allowed. After truncating the lattice, this situation results in directive radiation because the tangential component of the wavevector must be continuous at the EBG–vacuum interface [4]. The constant frequency dispersion diagram for the working point just above the bandgap better clarifies the underlying physical mechanism. This kind of diagram is shown in Fig. 3(a) along with the 3-D plot of the air band; the shaded cones at the bottom of the picture represent the angular ranges of allowed Bloch waves for $k_0 p/\pi = 0.545$, making the focusing effect visually clear. From Fig. 2, it can be noticed that, for $k_0 p/\pi = 0.365$, Bloch waves with either $k_x = 0$ or $k_y = 0$ are allowed in the dielectric band too, where the lower gray line crosses the "X" point. Such working condition is shown in Fig. 3(b); in this case, Bloch waves propagating in different directions are also allowed in the lattice. Given a current source embedded in the lattice, it has been shown that its position plays an important role in directive antennas based on Bloch waves [18]. The modal analysis of the infinite 2-D lattice allows us to intuitively grasp this role, but it cannot provide much physical insight and also information about the effects of the lateral truncation on the radiation patterns.

The choice of the lattice parameters is a tradeoff between several factors. As far as the dielectric permittivity

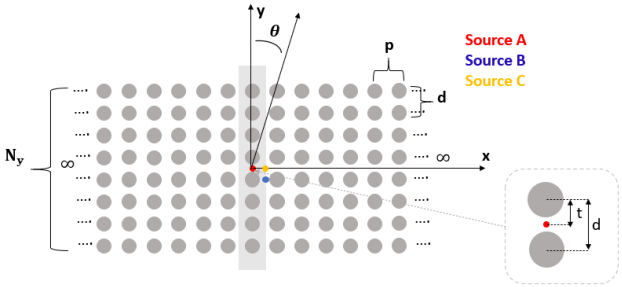

Fig. 5. 2-D EBG structure consisting of a finite number N_y of periodic chains spaced d along the y-direction, each one of them having an infinite number of 2-D circular rods with radius r and spaced p along the x-direction; $r = 0.35p$, $d/p = 1$, and relative dielectric constant $\epsilon_r = 11.7$. Three different positions of the source within the unit cell, indicated as a light gray shadowed region, are marked in red, blue, and yellow. Here, θ is the angle measured from broadside.

is concerned, beside its impact on the performance of the specific lattice-based device, the availability, cost, and machinability of materials also play an important role. Fig. 4 shows a parametric plot of the bandgap versus the ratio r/p for three different relative dielectric constants. With low values of r/p, the bandgap width increases, but the size of the device increases too for a fixed working frequency. In a previous work [18], the lattice parameters of Fig. 2 were deemed as a good compromise and will also be adopted here.

III. Modal Analysis of a Stack of a Finite Number of Periodic Chains of Circular Cylinders

In this section, we operate a detailed modal analysis of the open waveguide shown in Fig. 5 composed of a stack of a finite number of periodic chains of dielectric cylinders of infinite length. Here, the concept of a waveguide of finite width along the y-direction and periodic along the x-direction is explored in such kind of EBG dielectric structures. The basic advantage of the adopted model, with respect to that described in Section II, consists in the possibility of rigorously accounting for radiation losses in the free space above and below the stack of periodic chains, by properly considering leaky modes propagating along the x-axis of the waveguide. The proposed waveguide, which is invariant with respect to the z-direction, supports the propagation of both TE and TM, with respect to both the y- and x-directions, bound and leaky modes. However, since we are interested in the radiative features of the lattice structure when excited by an electric line source extending along the z-direction, we will consider here only TE modes.

A. LSs Technique for Multilayered Periodic Chains

In the source-free case of the modal analysis, the modal field in a periodic waveguide composed of a number N_y of periodic chains, as shown in Fig. 5, can be expressed in terms of an infinite series of space harmonics, each having a given complex propagation wavenumber $k_{xm} = k_x + k_m$, with $k_x = \beta - j\alpha$, $k_m = 2\pi m/p$, and $m = 0, \pm 1, \pm 2, \ldots$ Each space harmonic propagates along x with a different phase constant $\beta_m = \beta + 2\pi m/p$, but with the same attenuation constant α [24], [46]. The mth space harmonic along the transverse y-axis in free space behaves as $e^{-jk_{ym}|y|}$, where $k_{ym} = (k_0^2 - k_{xm}^2)^{1/2}$ is the relevant wavenumber. A dispersion equation for the eigenmodes can be written in the following form, by following the approach in [37] and [42]:

$$\det[\mathbf{I} - \mathbf{D}(k_x) \cdot \mathbf{R}_N(k_x) \cdot \mathbf{D}(k_x) \cdot \mathbf{R}_{N_y-N}(k_x)] = 0 \qquad (3)$$

with

$$\mathbf{D}(k_x) = [\exp(-jk_{ym}d)] \qquad (4)$$

where $\mathbf{D}(k_x)$ represents the transverse traveling wave behavior of each space harmonic between two adjacent layers of periodic chains along the y-axis spaced by a distance d (Fig. 5), $\mathbf{R}_N(k_x)$ and $\mathbf{R}_{N_y-N}(k_x)$ are the generalized reflection matrices for the N-layered and $(N_y - N)$-layered periodic structures, respectively, with $N = 1, 2, \ldots, N_y - 1$, and $\mathbf{I}$ is the unit matrix. The generalized reflection matrices $\mathbf{R}_N(k_x)$ and $\mathbf{R}_{N_y-N}(k_x)$ are derived by using the LSs technique combined with the transition matrix (T-matrix) approach [47]. The LS, which is expressed as a sum of spectral and spatial higher order series, is accurately calculated using the Ewald method for the complex wavenumber k_{xm} [42]. The proper $\mathrm{Im}[k_{ym}] \leq 0$ and improper $\mathrm{Im}[k_{ym}] \geq 0$ nature of the modal field, determining the transverse field behavior of the mth space harmonic, is considered by suitably choosing the appropriate square root determination for $k_{ym} = (k_0^2 - k_{xm}^2)^{1/2}$ [24], [46].

B. Brillouin Diagram

The Brillouin diagram, shown in Fig. 6 for the case where $N_y = 8$, illustrates the dispersive behavior of the space harmonics as a plot of the normalized frequency $k_0 p/\pi$ versus the normalized phase constant $\beta p/\pi$, where β represents the phase constant along x of any particular space harmonic [46]. At low frequency, below the light line, reported as a red dashed line, we observe eight bound dielectric modes (DMs), numbered from 0 to 7 by increasing frequency, one for each of the eight periodic chains of the structure; the relevant phase constants ($m = 0$ harmonics) with positive group velocity (*forward* kind of propagation) are indicated as black solid lines. We note that the first (fundamental) mode, i.e., DM_0, does not have cutoff frequency, as was also observed for the TE mode in the single periodic chain [37], while the other seven forward DMs show distinct cutoff frequencies. Between $0.440 < k_0\, p/\pi < 0.520$, a closed stopband regime occurs for all the bound DMs, where the modal wavenumber is complex and the normalized phase constants have a pure vertical behavior versus frequency at $\beta p/\pi = 1$ (see the gray shadowed region in Fig. 6). Here, the propagation in the waveguide is not allowed for all the eight DMs. For $k_0 p/\pi > 0.52$, the eight DMs of the stack of periodic chains present a second passband region where the wavenumbers are again proper and real and the propagation is of the *backward* kind (the phase constants of the first three backward dielectric modes (BDMs), $m = -1$ harmonics with negative group velocities, are shown as black thin solid lines and are numbered from 0 to 2 consistently with the forward DMs at lower frequencies). At higher frequencies, eight forward bound air modes (AMs) also

exist (the phase constants of only the first three AMs, $m = 0$ harmonics with positive group velocities, are here shown as black solid lines and numbered from 0 to 2). We observe that the phase constants of these BDMs and AMs cross each other with different negative and positive slopes; very narrowband coupling phenomena can occur [33], which, however, are not investigated in this article.

To the left of the light line, we can observe the fast-wave region. When a leaky mode lies within this region, the mode is *physical* [24], [25], and if properly excited by a specific source, it could produce directive radiative phenomena (we are interested here only in physical leaky modes). We note that each forward or backward bound mode shown in the Brillouin diagram presents an improper or proper, respectively, leaky-wave branch, except for the first dominant mode at low frequencies, which does not have cutoff frequency. In particular, also the second and third DMs at low frequencies present improper leaky-wave branches, but they are not physical, since the relevant phase constants do not cross the light line, and hence, they are not shown in Fig. 6. The remaining five modes of the first set of bound DMs have all improper leaky-wave branches, originating below their cutoff frequency. For each of these modes, a spectral gap occurs [48], not reported in this figure but described in Section III-D for the AM_0, below which each complex solution enters the fast-wave region, as shown by the red lines corresponding to the phase constants ($m = 0$ harmonic) of these forward leaky modes. As concerns the modes above the stopband region, three improper leaky AMs are shown in the Brillouin diagram as analytic continuations of the reported forward bound AMs. At higher frequencies, backward leaky modes exist as analytic continuations of the three bound BDMs shown in Fig. 6; however, they are not reported here, since in that frequency region, the structure is highly multimodal and the radiative features are not of interest for the present study.

In the Brillouin diagram, two horizontal dashed lines are reported, indicating the two frequencies where focused radiation at broadside is expected on the basis of the investigation performed in Section II. We observe that the line at $k_0 p/\pi = 0.365$ intersects one improper leaky DM and seven bound DMs, whereas at $k_0 p/\pi = 0.545$, three improper leaky AMs and two bound BDMs can propagate. We note that the band diagram in Section II predicted the former result because Bloch waves propagating in different directions of the photonic crystal were allowed [see Fig. 3(b)], while at the highest frequency, only focused radiation at broadside was expected [see Fig. 3(a)], which can be related to the presence of leaky modes of the open waveguide, but not of bound modes in the backward regime.

The highly multimodal behavior observed for such kind of lattice waveguide could create potential difficulties in optimizing focused leaky-wave radiation. In fact, a desirable feature of LWAs is related to the possibility of exciting, at a given operating frequency, a single dominant leaky mode in the absence of any other bound and leaky modes supported by the structure. The presence of more than one leaky mode would produce undesired multiple beams pointing in different directions, whereas the simultaneous excitation of bound

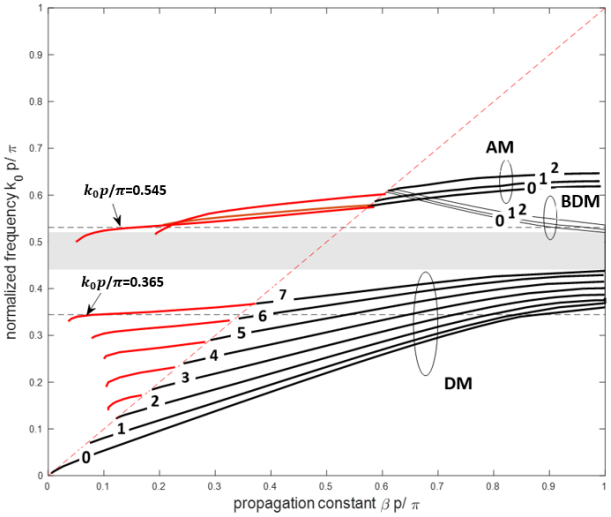

Fig. 6. Brillouin diagram for the $m = 0$ and $m = -1$ space harmonics of the TE bound and leaky modes of the structure of Fig. 5. Bound DMs and AMs are indicated as black thick solid lines. Bound BDMs are indicated as black thin solid lines. Physical improper leaky DMs and AMs are shown as red thick solid lines. The light line is shown as a red thin dashed line.

modes, in addition to leaky modes, would highly decrease the efficiency of the LWA or produce unwanted spurious radiation at the truncation in practical scenarios. Unfortunately, for this kind of lattice geometries, it is not possible to decrease the number of propagating modes, which increases with the rod numbers N_y, and obtain a purely monomodal leaky-wave propagation. However, suitable choices of the source position could be made to reduce the undesired effects. In order to ascertain this subtle issue, a deep analysis of the modal fields for all the solutions reported in the Brillouin diagram of Fig. 6 will be performed in Section III-C.

C. Modal Field Configurations and Symmetries

The study of the modal field configuration is here performed in order to optimize the leaky-wave radiation in multimodal structures. The goal of our analysis is to understand whether it is possible to properly excite only one leaky mode, e.g., around the normalized frequencies $k_0 p/\pi = 0.365$ and $k_0 p/\pi = 0.5452$, in absence of any other bound and/or leaky mode. Since an electric line source along the z-direction will be here considered as an idealized feeder, in this section, the z-component of the electric modal fields of the TE Bloch waves propagating along the x-direction will be investigated.

In Fig. 7(a), a color plot of the amplitude of the electric modal field within the chosen unit cell is shown for the first eight bound DMs when $\beta p/\pi = 0.4$ at the normalized frequencies indicated. We can observe an alternation of even and odd modes of increasing order, presenting a strong maximum or a zero, respectively, between the central cylinders in the middle of the unit cell, corresponding to perfect magnetic conductor (PMC) or perfect electric conductor (PEC) symmetry in the $y = 0$ plane, respectively. Furthermore, the local maxima of the fields are obtained in the middle of each dielectric cylinder, as typically occurs for the modes of a 2-D dielectric lattice in the *dielectric* band [41]. Finally, we note that DM_7 and, hence, the relevant improper leaky-wave branch

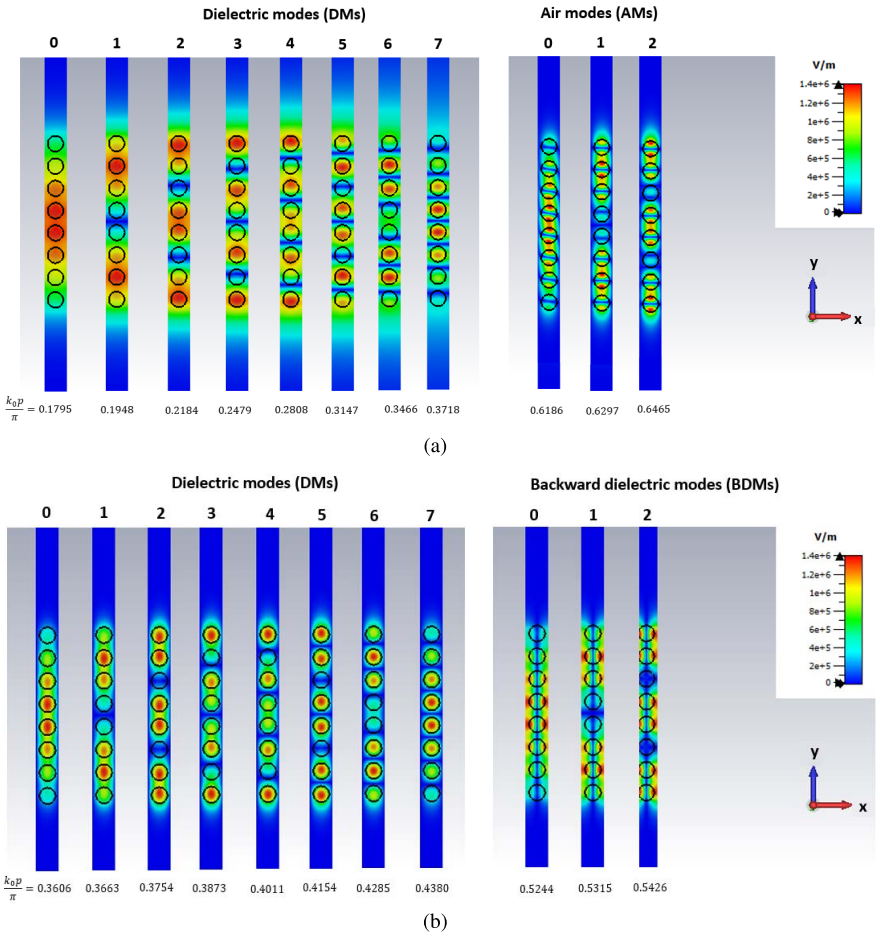

Fig. 7. Modal field configurations (magnitude of E_z-field) of (a) first eight forward DMs for $\beta p/\pi = 0.4$ and the first three AMs for $\beta p/\pi = 0.95$ and (b) first eight forward DMs and the first three BDMs for $\beta p/\pi = 1$.

cannot be excited by a source in position A, as shown in Fig. 5, since a PEC symmetry is present in $y = 0$. DM_7 can instead be excited by a source in position B, where a local maximum of the electric field is found. However, the latter position of the source will inevitably excite almost all the other bound DMs, thus reducing the radiation efficiency and increasing possible diffraction effects at the lateral truncation in a practical LWA.

At higher frequency, above the stopband, we have forward AMs and BDMs. As concerns the former, in Fig. 7(a), the modal fields of the first three modes (AM_0, AM_1, and AM_2) are shown. The global trend of the modal fields observed for DM_0, DM_1, and DM_2 is preserved, i.e., even and odd modes alternate with increasing oscillations. However, we can observe that in the AMs, the local maxima of the fields are placed in the *air* region between each cylinder, whereas deep minima are placed in the middle of each cylinder. Since the leaky modes are assumed to preserve the same modal configurations of the corresponding bound branches, in order to excite the improper leaky AM_0 at $k_0 p/\pi = 0.5452$, the line source should be placed in position A in Fig. 5, where a PMC symmetry is present. Coupling with the improper leaky AM_1 will be hence totally minimized since a PEC symmetry plane in $y = 0$ is noticed in Fig. 7(a). However, the improper leaky AM_2 will be excited by such source and, in case, its contribution to the radiated field should be considered. At the frequency $k_0 p/\pi = 0.5452$, as was noticed commenting Fig. 6, two BDMs (i.e., BDM_0 and BDM_1) are also present. However, the source in position A will not excite any of them, as explained in the following description of the modal field configurations at the stopband edges.

As concerns the modal field configuration before and after a stopband region, we note that when considering a symmetric unit cell, e.g., with respect to the plane $x = 0$, as in Fig. 5, the fields at the band edges are necessarily either symmetric (S) or antisymmetric (AS) with respect to the same plane [49], [50]. In our study, the lowest edge of the stopband is of the S type with the transverse electric field of the Bloch mode equal to zero at the reference unit-cell planes [see DM field configurations in Fig. 7(b)]. Indeed, the highest edge is of the AS type, with the transverse electric field maximum at the unit-cell borders and equal to zero at the center of the unit cell (see the odd symmetry with respect to the plane $x = 0$), as shown in Fig. 7(b) for the BDM_0, BDM_1, and BDM_2. Hence, at the normalized frequency $k_0 p/\pi = 0.5452$, the reaction between these BDM fields and the z-directed electric line source in position A is negligible. This is a very important result, since due to the symmetry of the structure, it is possible to excite at $k_0 p/\pi = 0.5452$ the leaky AM_0 (and in case AM_2) in the absence of any other bound modes, thus simplifying the design process of LWAs based on such EBG structures.

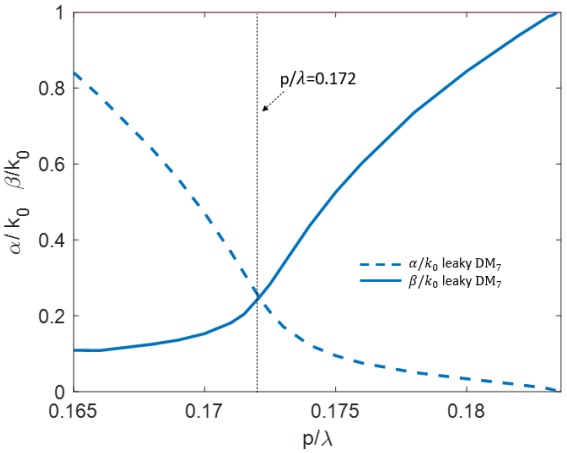

Fig. 8. Dispersion diagram for the leaky DM_7. Normalized phase constant β/k_0 is shown as a blue solid line. Normalized attenuation constant α/k_0 is shown as a blue dashed line.

D. Leaky-Wave Solutions

In this section, the dispersion behaviors of the normalized phase and attenuation constants of the leaky modes, which could be responsible for focused radiation, at the normalized frequencies individuated in Sections II and III-B, are reported. In Fig. 8, the normalized phase and attenuation constants, β/k_0 and α/k_0, respectively, of the $m = 0$ harmonic for the leaky DM_7 versus normalized frequency p/λ are shown. We note that the condition for maximum radiation power density at broadside, i.e., $\beta = \alpha$, which corresponds to the main beam on the verge of splitting into two separate beams (beam-splitting condition) [51], occurs at $p/\lambda = 0.172$. Here, a quite high value of the normalized attenuation constant, i.e., $\alpha/k_0 \simeq 0.25$, is obtained.

In Fig. 9(a), the normalized phase β/k_0 ($m = 0$ harmonic) and attenuation α/k_0 constants of the leaky AM_0 and AM_2 are plotted as a function of the normalized frequency (we did not show the behavior of the leaky AM_1, since with the source in position A, we can avoid its excitation). We observe that the normalized frequency corresponding to the maximum radiated power at broadside for the AM_0, i.e., at which the condition $\beta = \alpha$ is satisfied, is $p/\lambda = 0.265$. At this frequency, the normalized attenuation constant of the leaky AM_2 is about six times higher than that of the leaky AM_0, and hence, its contribution to broadside radiation can be neglected or is not dominant. However, the value of the normalized attenuation constant of the AM_0 is quite high ($\alpha/k_0 \simeq 0.252$) to give rise to highly directive radiation at broadside. Finally, in Fig. 9(a), a detail of the spectral gap [48] between the improper leaky branch of the AM_0 and the relevant real proper solution, corresponding to the bound AM_0, is reported, including real improper branches and the splitting point (SP); a significant similarity with the transition region reported in other kind of 1-D periodic open structures, with 2-D geometry, is observed [52].

In order to obtain lower values of the attenuation constant for the leaky AM_0 and, hence, to improve the directivity, the number N_y of periodic chains needs to be increased, as can be inferred by the discussion on the focusing properties

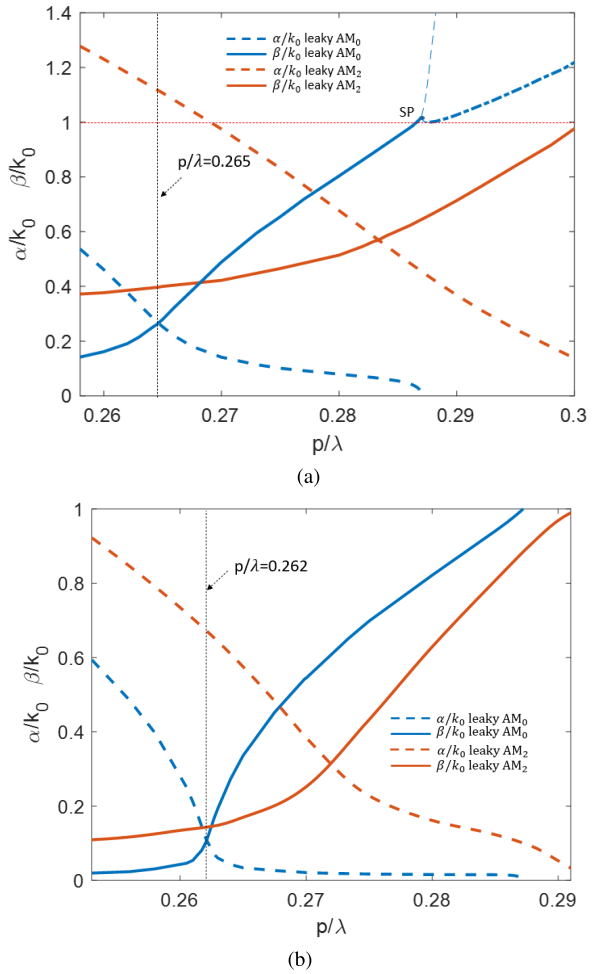

Fig. 9. Dispersion diagrams for the leaky AM_0 and the leaky AM_2. Normalized phase constant β/k_0 of the AM_0: blue solid line, complex improper solution; thin blue dashed line, improper real branches; blue dashed-dotted line, proper real solution. Normalized attenuation constant α/k_0 of the leaky AM_0: blue dashed line. Normalized phase and attenuation constants of the leaky AM_2 are shown as red solid and dashed lines, respectively. The light line is shown as a red dotted horizontal line. In (a), the case of the structure with $N_y = 8$. In (b), $N_y = 16$.

of the 2-D lattices [4], [5], which are infinite in both the x- and y-directions, reported in Section II. The resulting dispersive behavior and Brillouin diagram are quite similar to those described in Sections III-B and III-C, but with a number of the DMs and AMs that increase with that of the periodic chains. In Fig. 9(b), the dispersion behavior of the leaky AM_0 and AM_2 for a structure as in Fig. 5 but with a stack of 16 periodic chains is shown. Quite low values of the attenuation constant are obtained for the dominant leaky AM_0 at the broadside beam-splitting normalized frequency of $p/\lambda = 0.262$ ($\alpha/k_0 \simeq 0.114$) that could allow for highly directive radiated beam, as we will verify in Section IV.

IV. Radiation Features of a Line Source Embedded in 2-D Dielectric Lattices: Infinite and Truncated Structures

In this section, accurate derivations of the far fields radiated by an electric line source embedded in the EBG lattice waveguide are provided, for infinite and truncated structures,

and the results obtained through the full-wave simulations with CST, the LSs technique, and the CWA are presented. In particular, as concerns the infinite structure, the spectral-domain formulation of the LSs approach [42], [53] allows for the rigorous evaluation of the residue contributions of the excited leaky modes to the aperture antenna fields and hence to the radiated fields.

A. Spectral-Domain Representation of the Field Excited by a Line Source Embedded in a Stack of a Finite Number of Periodic Chains

In this section, the field generated by an aperiodic electric line source, embedded in a stack of a finite number of periodic chains of dielectric cylinders and located within the unit cell (shown as a shadowed vertical region in Fig. 5), is derived. The line source, expressed as $\mathbf{J}(x, y) = \delta(x)\delta(y)\mathbf{z}$, is transformed into an infinite periodic array of linearly phased line sources in the spectral domain [43], [54]. For each of the spectral components, the periodic line sources excite a set of weighted space-harmonic fields. The spectral response of the EBGs to the line source excitation is calculated using the LSs technique [42], [53]. The scattering amplitudes $\mathbf{c}^+(k_x)$ and $\mathbf{c}^-(k_x)$ of the space-harmonic fields transmitted in the upper and lower regions, respectively, are expressed through the incident spectral amplitudes $\mathbf{s}(k_x)$ of the infinite periodic line sources using the following relations [54]:

$$\begin{aligned}\mathbf{c}^+ &= \mathbf{F}_1 \times \{[\mathbf{I} - \mathbf{\Lambda} \times \mathbf{R}_2 \times \mathbf{\Lambda} \times \mathbf{R}_1]^{-1} \times \mathbf{\Lambda} \\ &\qquad \times \mathbf{R}_2 \times \mathbf{\Lambda}_2 \times [\mathbf{I} + \mathbf{\Lambda}_1 \times \mathbf{R}_1 \times \mathbf{\Lambda}_1] + \mathbf{\Lambda}_1\} \cdot \mathbf{s} \\ &= \mathbf{Q}^+ \cdot \mathbf{s} \qquad (5)\\ \mathbf{c}^- &= \mathbf{F}_2 \times \{[\mathbf{I} - \mathbf{\Lambda} \times \mathbf{R}_1 \times \mathbf{\Lambda} \times \mathbf{R}_2]^{-1} \times \mathbf{\Lambda} \\ &\qquad \times \mathbf{R}_1 \times \mathbf{\Lambda}_1 \times [\mathbf{I} + \mathbf{\Lambda}_2 \times \mathbf{R}_2 \times \mathbf{\Lambda}_2] + \mathbf{\Lambda}_2\} \cdot \mathbf{s} \\ &= \mathbf{Q}^- \cdot \mathbf{s} \qquad (6)\end{aligned}$$

with

$$\mathbf{s}(k_x) = \left[\frac{2}{pk_{ym}}\right] \qquad (7)$$

$$\mathbf{\Lambda}_1(k_x) = \exp[-jk_{ym}t]\delta_{mm'} \qquad (8)$$

$$\mathbf{\Lambda}_2(k_x) = \exp[-jk_{ym}(d-t)]\delta_{mm'} \qquad (9)$$

$$\mathbf{\Lambda}(k_x) = \exp[-jk_{ym}d]\delta_{mm'} \qquad (10)$$

where $\mathbf{R}_1(k_x)$ and $\mathbf{F}_1(k_x)$ and $\mathbf{R}_2(k_x)$ and $\mathbf{F}_2(k_x)$ are the generalized reflection and transmission matrices of the upper and lower EBG structures with respect to the line source, $\mathbf{\Lambda}_1$, $\mathbf{\Lambda}_2$ and $\mathbf{\Lambda}$ are the diagonal matrices that characterize the phase shift of each space harmonic along the y-axis between the line source and the centers of the nearest layers of the upper and lower EBGs, with t and $d - t$ the relevant separation distances (see the inset in Fig. 5), and $\delta_{mm'}$ is the Kronecker delta. We note that if the source is located at the global origin of the unit cell, then $t = d/2$ and $\mathbf{\Lambda}_1(k_x) = \mathbf{\Lambda}_2(k_x)$. In addition, it should be noted that the upper and lower EBGs can be shifted along the x-axis with respect to the line source. The matrices, which define the phase shift of the space harmonics along the x-axis within the unit cell, are included in the expressions of the generalized reflection $\mathbf{R}_1(k_x)$ and $\mathbf{R}_2(k_x)$ and transmission $\mathbf{F}_1(k_x)$ and $\mathbf{F}_2(k_x)$ matrices. Since the scattering amplitudes in the upper and lower regions are rigorously defined, the fields $E_z^{\pm}(x, y)$ in the upper ("+" sign) and lower ("−" sign) regions are obtained in the following form [54]:

$$E_z^{\pm}(x, y) = \frac{p}{2\pi}\int_{-\pi/p}^{\pi/p} dk_x \left[\sum_{m=-M}^{M}\sum_{n=-N}^{N} Q_{mn}^{\pm} \cdot s_n\right] \times e^{-jk_{xm}x \mp jk_{ym}y} \qquad (11)$$

where N and M are the truncation numbers of the columns and rows of the matrices in (5) and (6) (without loss of generality, we take the truncation number of the matrices to be the same $N = M$). In the far zone, applying the method of stationary phase [55], the radiated field from the localized line source could be written as follows [54]:

$$E_z^{\pm}(\rho, \theta) = \frac{pk_0}{\sqrt{2\pi}}\cos\theta \exp\left(j\frac{\pi}{4}\right) \times \frac{\exp(-jk_0\rho)}{\sqrt{k_0\rho}}\left[\sum_{n=-N}^{N} Q_{0n}^{\pm} \cdot s_n\right]_{k_x = k_0\sin\theta} \qquad (12)$$

where $\rho = \sqrt{x^2 + y^2}$, θ is the observation angle, and only the $m = 0$ harmonic is fast.

Although the computation of (11) along the integration path in the first Brillouin zone of the complex k_x plane, i.e., the strip of the k_x complex plane defined by $-\pi/p < \mathrm{Re}(k_x) < \pi/p$, completely determines the excited aperture field on the periodic structure, i.e., the field at the interface between free-space and EBG waveguide, it is very convenient to carry out a *spectral* decomposition of this aperture field. Such decomposition allows for a deeper physical insight into the excitation of the discrete spectrum (which accounts for the proper modes) as well as the continuous spectrum (associated with reactive and/or radiative effects) [39], [40]. The latter can be further expressed, by means of a *nonspectral* representation of the excited field, as the sum of the residue contributions of the captured (physical) proper and improper leaky poles of the integrand in (11) and the contribution of the integral around the branch point, which constitutes the residual-wave field, i.e., the direct radiation from the line source [38], [56]. In the following, leaky-wave far-field normalized patterns will be shown by also considering the simultaneous contribution of two leaky modes, each weighted by the respective residue.

B. Radiative Features of the Infinite Structures

In this section, we describe the radiative features of the structure of Fig. 5, which is infinite along the x-direction and composed of a finite number of cylinders in the orthogonal y-direction. The exact total far field excited by an embedded electric line source, parallel to the axes of the rods (i.e., the z-direction), is obtained using both the semianalytical spectral-domain approach described in Section IV-A and CST Studio Suite, simulating a single unit cell in a periodic environment and applying reciprocity [57]. Normalized leaky-wave radiation patterns obtained considering only the dominant leaky-wave or further higher order leaky-wave

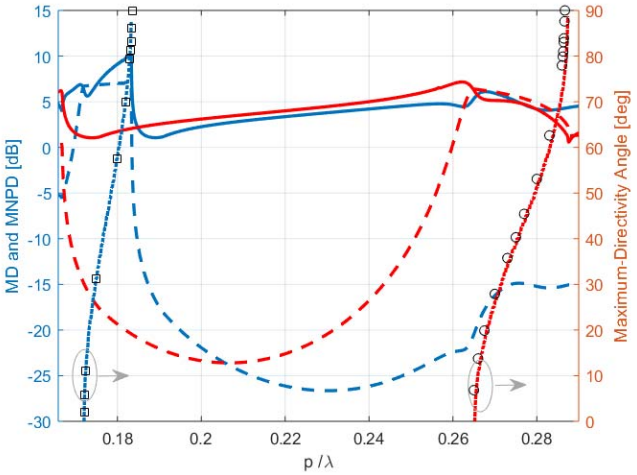

Fig. 10. Plot of the MD (solid line), MNPD (dashed line), and angle of MD (dotted line) as a function of the normalized frequency p/λ for the infinite waveguide in Fig. 5 with N_y =8. Results for the source in positions A and B are indicated in red and blue, respectively. Theoretical leaky DM_7 and AM_0 radiation angles are also shown with square and circle black markers, respectively.

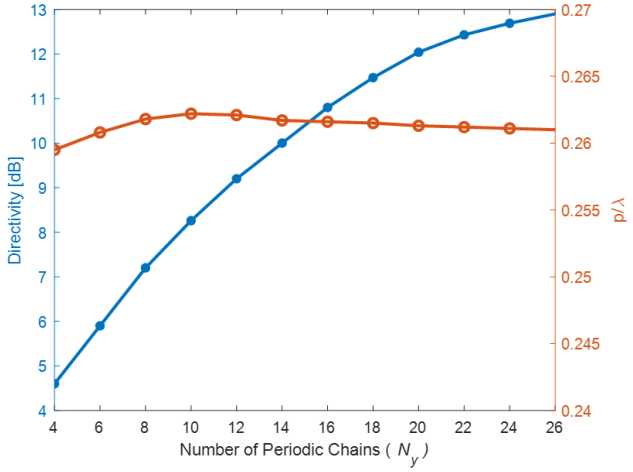

Fig. 11. Plot of the maximum value of the directivity at broadside and the normalized frequency p/λ at which it is obtained versus the number of periodic chains N_y for the source in position A.

contributions, suitably weighted by the relevant excitation coefficients, as introduced in Section IV-A, will be shown to validate the proposed approach.

The directive radiative features of a lattice structure composed by eight periodic chains are reported in Fig. 10 as a function of the normalized frequency p/λ. In particular, the behaviors of the maximum directivity (MD), evaluated as

$$\mathrm{MD} = \max_{\theta} \frac{|E_z(\theta)|^2}{\frac{1}{2\pi}\int_0^{2\pi} |E_z(\theta')|^2 d\theta'}, \tag{13}$$

and of the maximum normalized power density (MNPD), defined as the maximum angular power density of the EBG lattice structure divided by the relevant isotropic quantity E_{fs} for the line source in free space

$$\mathrm{MNPD} = \max_{\theta} \frac{|E_z(\theta)|^2}{|E_{fs}|^2}, \tag{14}$$

are considered. Two regions of high directivity are individuated, one in the frequency region just below the lower edge of the stopband and the other slightly above, when the electric line source is in positions B and A, respectively. The angle θ, corresponding to MD and MNPD, scans from broadside to endfire by increasing frequency in both cases. Maximum broadside power enhancement values (with respect to the same line source in free space) are obtained at the broadside beam-splitting normalized frequencies, i.e., when $\beta = \alpha$, and are equal to 6.4 dB at $p/\lambda = 0.265$ and to 6.7 dB at $p/\lambda = 0.172$, for the source in positions A and B, respectively. We note that the directive radiative regions are consistent with the radiative features of the leaky modes DM_7 and AM_0, whose theoretical angles of radiation, obtained by using the well-known formula $\theta = \sin^{-1}\sqrt{(\beta_0/k_0)^2 - (\alpha/k_0)^2}$ [25], are in perfect agreement with those of MD. As concerns the highest MDs at broadside, the values of 7.2 dB at $p/\lambda = 0.262$ and 6.8 dB at $p/\lambda = 0.1705$ are obtained, where $\beta \simeq 0.52\alpha$ in both cases, according to the condition for broadside beamwidth (BW) minimum reported in [27, eq. (46)].

The maximum value of the directivity at broadside for the source in position A is shown in Fig. 11 as a function of the number of rods along the y-direction. It can be observed that the directivity increases with N_y, as predicted by the decreasing behavior of the values of the normalized attenuation constants for the dominant leaky AM_0 reported in Section III-D. Furthermore, the normalized frequency at which the maximum value of the directivity at broadside is obtained for different values of N_y is almost constant since it is related to the higher edge of the complete bandgap of the infinite 2-D lattice described in Section II.

The far-field radiation patterns evaluated at the frequencies of maximum broadside power density are here reported for the infinite waveguide with $N_y = 8$. In Fig. 12, the polar plot of the normalized far field excited by the source placed in position B at $p/\lambda = 0.172$ is obtained by simulating a single unit cell in a periodic environment with CST and applying reciprocity and compared with the normalized leaky-wave far-field patterns of the DM_7. We can observe that due to the asymmetric position of the source, the far fields above and below the infinite waveguide are different. The agreement with the leaky-wave far field is excellent, in particular below the stack of periodic chains. However, we note that the simultaneous propagation and excitation of the other bound DMs, as observed in Section III-C, make LW radiation poorly efficient in this frequency region.

In the following, radiation features for the source in position A are presented and discussed. Only angles, measured from the positive y-axis, ranging from $-90°$ to $+90°$, through $0°$, will be shown since the examined structure is symmetric with respect to the $y = 0$ plane. In Fig. 13, the exact total normalized far field at $p/\lambda = 0.265$ obtained with the LSs technique by applying (12) and by simulating a single unit cell in a periodic environment with CST and applying reciprocity is compared with the normalized leaky-wave far-field patterns of the AM_0 alone and with that obtained by considering both the AM_0 and AM_2, each weighted by the respective residue contribution. First, the total far fields obtained with the semianalytical approach based on the LSs and the full-wave

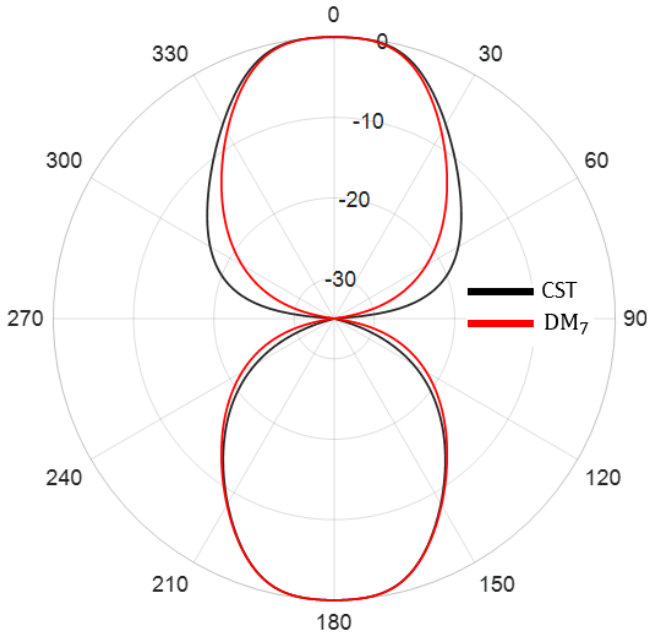

Fig. 12. Polar plot of the normalized far field excited by the source in position B. Comparison between the CST total field and the leaky DM_7 field for $p/\lambda = 0.172$.

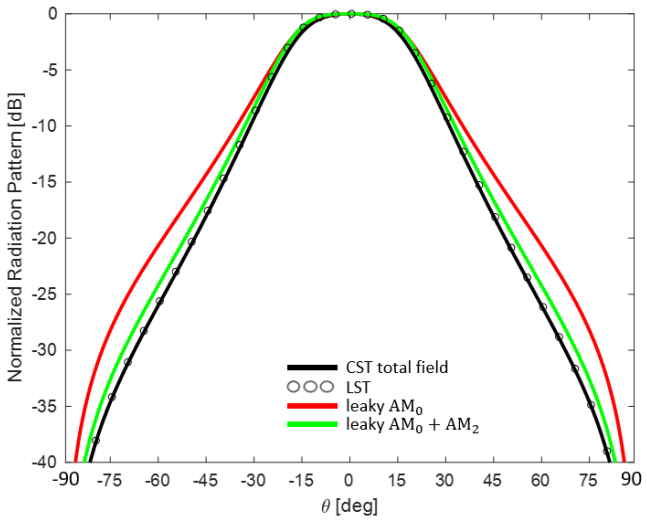

Fig. 13. Comparison between the leaky AM_0, leaky $AM_0 + AM_2$, and LS technique (LST) and CST total far-field normalized radiation patterns for $p/\lambda = 0.265$.

software CST are in perfect agreement. Then, we can observe that the leaky AM_0 alone provides the dominant contribution to the total far field, but the agreement is not excellent. Finally, if we consider both the leaky AM_0 and AM_2 excited by the source in position A, weighted by the relevant residues, a definitively better agreement with the total field is reached.

In Fig. 14, the far-field radiation patterns for the infinite lattice structures with $N_y = 16$ are shown at the frequency of maximum broadside power density, i.e., $p/\lambda = 0.262$. An MD at broadside of 10.8 dB, which is considerably higher than that observed for $N_y = 8$, is obtained at a slightly lower normalized frequency $p/\lambda = 0.2616$, where $\beta \simeq 0.54\alpha$. Also, in this case, in order to improve the agreement between the leaky-wave radiation patterns and the total field, the weighted

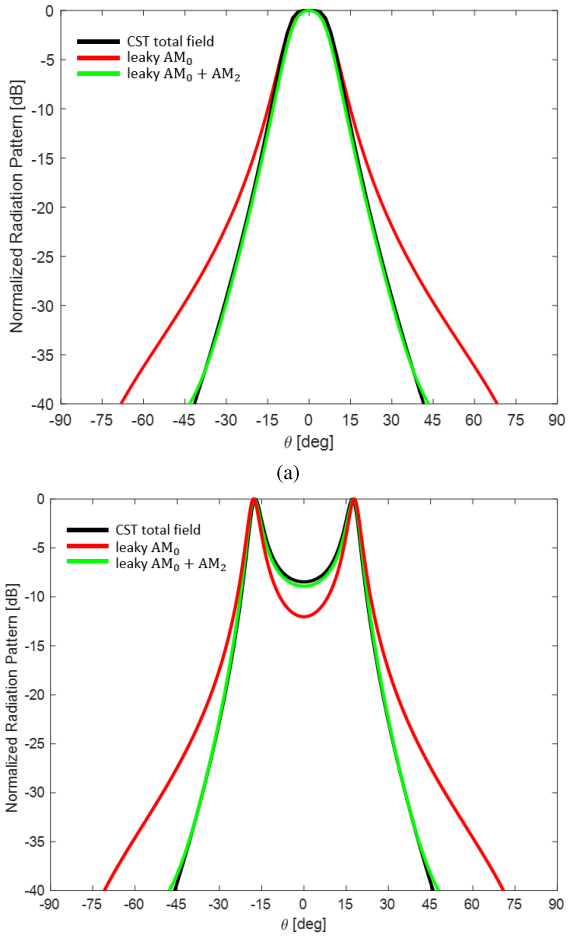

Fig. 14. Normalized radiation patterns: (a) Comparison between the leaky AM_0, leaky $AM_0 + AM_2$, and CST total far fields for the structure with $N_y = 16$ and $p/\lambda = 0.262$. (b) Comparison between the leaky AM_0, leaky $AM_0 + AM_2$, and CST total far fields for the structure with $N_y = 16$ and $p/\lambda = 0.2646$.

contributions of both the leaky AM_0 and AM_2 need to be considered. An excellent agreement is observed for the highly directive main beam at the broadside beam-splitting normalized frequency $p/\lambda = 0.262$ and for the scanned symmetric beams pointing at $-19°$ and $+19°$ at $p/\lambda = 0.2646$.

As concerns the numerical efficiency of the adopted *ad hoc* software used for the analysis, we observe that when $N_y = 8$, the computation time to obtain the complex wavenumber per one frequency using [42] is about 0.07 s, and with a negligible additional time to produce the leaky-wave far field of the infinite structure, the computation time to obtain the radiation pattern of the infinite structure with LST is about 1.2 s, whereas that with CST by using reciprocity (unit-cell environment with the frequency-domain solver) is about 648 s. The tests have been performed on a 3.7 GHz Intel Xeon CPU with 16 GB RAM.

In Table I, the pointing angles (PAs), BWs, MNPD, and MD obtained with CST and PAs and BWs predicted by means of approximate analytical formulas based on leaky-wave theory [25] for the infinite structures with $N_y = 8$, $N_y = 16$, and $N_y = 24$ are reported at the indicated normalized frequencies. For the structure with $N_y = 24$, the value of

TABLE I
COMPARISON BETWEEN CST TOTAL FIELD AND LW THEORY FOR THE INFINITE STRUCTURES

	CST				LW Theory (AM_0 mode)	
	PA (deg)	BW (deg)	MNPD (dB)	MD (dB)	PA (deg)	BW (deg)
N_y=8						
p/λ=0.265	0	38	6.4	6.4	0	42.8
p/λ=0.1721	0	40	6.7	6.7	0	40.5
N_y=16						
p/λ=0.262	0	17	11.5	10.3	0	16.2
p/λ=0.2646	18	4.9	11.3	10.7	19	4.4
N_y=24						
p/λ=0.2614	0	8	11.18	11.18	0	7.43

the normalized attenuation constant at the broadside beam-splitting normalized frequency $p/\lambda = 0.2614$ is $\alpha/k_0 \simeq 0.04$, which is considerably lower than those observed for $N_y = 8$ and $N_y = 16$, i.e., $\alpha/k_0 \simeq 0.252$ and $\alpha/k_0 \simeq 0.114$, respectively, whereas the highest MD at broadside, equal to 12.6 dB, is obtained at $p/\lambda = 0.2613$ when $\beta \simeq 0.54\alpha$. We note that the radiation angles of the main beams and the -3 dB BWs are well predicted by the values of the normalized wavenumbers of the leaky AM_0, which can be thus used for the design of directive radiators based on such kind of EBG waveguides.

C. Radiative Features of Truncated Structures

The design of a typical LWA is based on the radiative behavior of a dominant leaky mode, which, once excited by a suitable source, should radiate at least 90% of the injected power before reaching the antenna truncation, where the remaining 10% of the power is lost (matched loads or absorbers are usually positioned at the antenna terminations) [24]. Based on the analysis performed in this article, we observed that EBG waveguides composed of a finite number of periodic chains of dielectric rods support leaky modes that fully characterize the relevant directive radiative features. In particular, the TE leaky AM_0 is able to model the radiation pattern of the infinite EBG waveguide when excited by an electric line source placed at the center of the unit cell (i.e., at position A in Fig. 5), as reported in Table I. Hence, laterally truncated structures of the type in Fig. 1(c) can be easily sized depending on the targeted radiation efficiency $\eta_r = P_{rad}/P_{in} = 1 - e^{-\alpha N_x p}$ [24], where P_{rad} and P_{in} are the radiated power and the initial power, respectively, and N_x is the number of rods along the x-direction for the waveguide in Fig. 5. It then results to:

$$N_x = -\ln(1-\eta_r)/(2\pi\,\hat{p}\hat{\alpha}) \tag{15}$$

where $\hat{p} = p/\lambda$ and $\hat{\alpha} = \alpha/k_0$.

The design approach proposed here has been implemented at a frequency belonging to the 5G millimeter-wave (mm-wave) bands since 5G technology can take great advantage from antennas based on low-loss dielectric materials. Silicon dielectric rods of relative permittivity considered equal to 11.7 [58], with $r = 1$ mm and aligned with a spatial period $p = 2.9$ mm, have been adopted for 2-D dielectric lattices radiating at broadside at 27.4 GHz for the structure

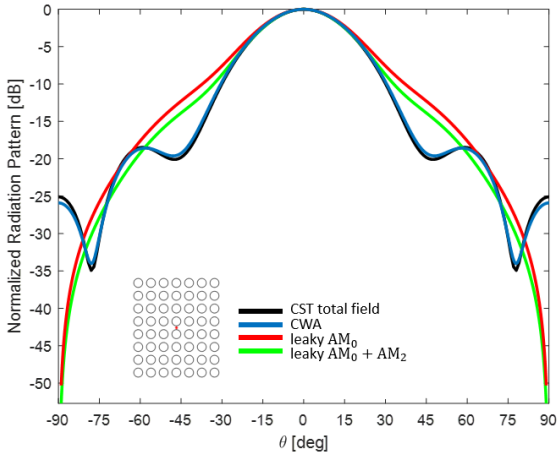

Fig. 15. Normalized radiation pattern for the truncated structure with $N_y = 8$ and $N_x = 7$: comparison between leaky AM_0, leaky $AM_0 + AM_2$, and CST and CWA total far fields, for a lattice with $r = 1$ mm and $p = 2.9$ mm at $f = 27.4$ GHz (i.e., $p/\lambda = 0.265$). Inset: geometry of the structure with the centered source (red spot).

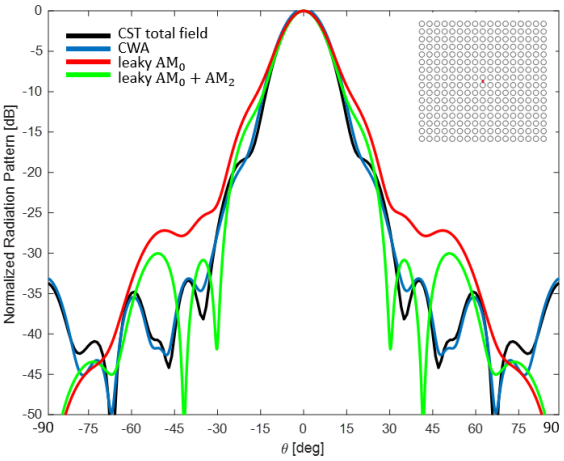

Fig. 16. Normalized radiation pattern for the truncated structure with $N_y = 16$ and $N_x = 17$: comparison between leaky AM_0, leaky $AM_0 + AM_2$, and CST and CWA total far fields, for a lattice with $r = 1$ mm and $p = 2.9$ mm at $f = 27.1$ GHz (i.e., $p/\lambda = 0.262$). Inset: geometry of the structure with the centered source (red spot).

with $N_y = 8$, i.e., at $p/\lambda = 0.265$, and at 27.1 GHz when $N_y = 16$, i.e., at $p/\lambda = 0.262$.

When the source is in position A, symmetric antennas will be considered and N_x will be chosen as the odd number that best fits (15) for the desired radiation efficiency. The EBG lattice structure composed of a stack of $N_y = 8$ periodic chains, with a total waveguide height of 22.3 mm, presents, for the leaky AM_0, a normalized attenuation constant $\alpha/k_0 \simeq 0.252$ at 27.4 GHz. Hence, a radiation efficiency $\eta_r \simeq 0.95$ can be obtained by selecting $N_x = 7$, corresponding to a lateral rod-to-rod total length of 19.4 mm, and placing the line source in the middle of the lattice. In Fig. 15, the exact total normalized far fields obtained with a semianalytical method based on the CWA [44] and the commercial EM software CST are in perfect agreement. The obtained directivity at broadside is equal to 7 dB. The leaky-wave patterns of both the leaky AM_0 and AM_2 and the leaky AM_0 alone are also plotted. The agreement between the full-wave and theoretical patterns is not always excellent, mainly due to the fact that the leaky-wave

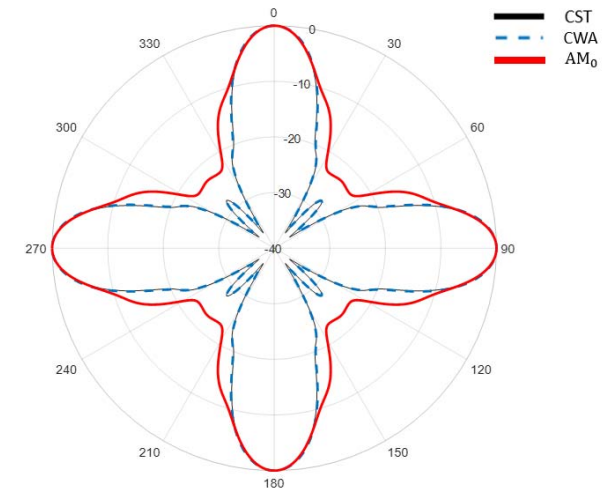

(a)

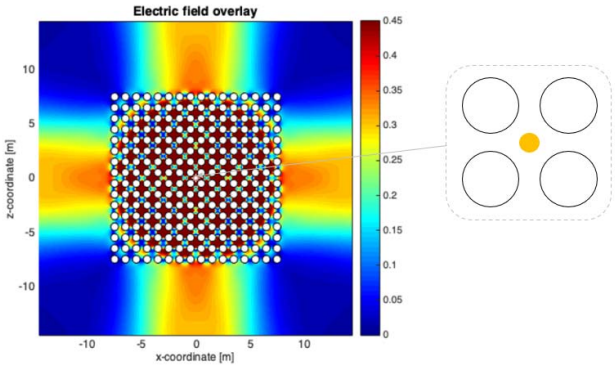

(b)

Fig. 17. (a) Polar plot of the normalized far field excited by the source in position C: comparison among the leaky AM_0, CWA, and CST total far fields for the structure with dimensions 45.5×45.5 mm ($N_x = N_y = 16$, $r = 1$ mm, and $p = 2.9$ mm) at $f = 27.1$ GHz (i.e., $p/\lambda = 0.262$). (b) Near-field amplitude pattern for the same structure. The source is positioned in the center of the structure as shown in the side picture.

theory only approximately accounts for the spurious diffraction at the edge of the structure (by adopting a physical-optics approach) and cannot include the spurious contribution given by the direct space-wave radiation from the source. However, the leaky AM_0 fully captures the main beam PA and the -3 dB BW. In Fig. 16, the far fields for the EBG lattice structure, composed of a stack of $N_y = 16$ periodic chains, with a total waveguide height of 45.5 mm, are presented. In this case, the leaky AM_0 normalized attenuation constant is $\alpha/k_0 \simeq 0.114$ at 27.1 GHz and a radiation efficiency $\eta_r \simeq 0.95$ is obtained by selecting $N_x = 17$, with a lateral total length of 48.4 mm. A directivity at broadside of 10.4 dB has been evaluated. A very good agreement is obtained between the exact full-wave normalized total fields and the theoretical patterns based on leaky-wave theory for both the leaky AM_0 and AM_2 and the leaky AM_0 alone, thus confirming our design approach. Table II shows the PAs, BWs, and MD obtained with CST and the PAs and BWs of the leaky AM_0 far field for the examined truncated structures, confirming the good agreement between the total and the leaky-wave far fields. Finally, the computation time to obtain the radiation pattern of the truncated structure, with $N_y = 16$ and $N_x = 17$, by using

TABLE II
COMPARISON BETWEEN CST AND LW FIELDS FOR THE TRUNCATED STRUCTURES

	CST			LW AM	
	PA (deg)	BW (deg)	MD (dB)	PA (deg)	BW (deg)
f=27.4 GHz N_y=8 N_x=7	0	33	7.0	0	35.8
f=27.1 GHz N_y=16 N_x=17	0	14.8	10.4	0	15.2

the CWA and CST (time-domain solver) is about 18.7 and 62 s, respectively, whereas for the leaky-wave far field, almost the same time as in the infinite structure is taken (i.e., about 0.1 s). The tests have been performed on a 3.7 GHz Intel Xeon CPU with 16 GB RAM.

We note that the intrinsic 2-D nature of the EBG structures studied in this article allows for considering the propagation of leaky modes along the x- and y-directions. In fact, when a finite number N_x of rods are considered, leaky modes propagating along the y-axis could also be excited if the source is properly placed. In order to exploit this peculiar characteristic, which is not typical of LWA based, e.g., on standard layered dielectric structures [59], but that has already been proposed for antenna applications in [18], a square structure with $N_x = N_y = 16$ excited at the center by a source in position C in Fig. 5 is investigated. Such a source couples with the leaky AM_0 propagating both along the x- and y-directions. The relevant normalized radiation patterns are shown in the polar plot in Fig. 17(a) where a good agreement between the AM_0 leaky contribution and the exact far fields obtained with both CWA and CST is observed, while an illustrative near-field plot is shown in Fig. 17(b).

V. CONCLUSION

The directive radiative features of an electric line source embedded in 2-D dielectric lattices have been investigated. These structures consist of square or rectangular arrays of circular dielectric cylinders of infinite length in free space, which are excited by an electric line source embedded within the lattice. A well-known design procedure to obtain directive radiation at broadside from such kind of structures is based on the analysis of the band diagrams of the infinite 2-D periodic lattices. By properly selecting the dielectric properties and the size of the cylinders as well as the period of the lattice, directive radiation can be obtained in the frequency range corresponding to the lower edge of the air band, just above the complete bandgap region of the EBG. A fully alternative approach, based on the thorough investigation of the bound and leaky modes of a waveguide composed of a stack of a finite number of periodic chains of circular dielectric cylinders, has shown here that this type of structure acts as an LWA, due to the propagation of a dominant leaky AM that can radiate a narrow beam at broadside as well as at any other angles. A detailed dispersive analysis of the dielectric and AMs supported by the selected open waveguides, considering bound modes both in the propagation and stopband regimes as well

as improper leaky modes, has shown the highly multimodal nature of such kind of EBG structures. The careful analysis of the relevant modal-field configurations revealed the existence of symmetry planes of the lattice structure and has allowed for choosing positions of the electric line source suitable to excite dominant leaky modes in the absence of any other bound mode.

Radiation patterns of infinite EBG structures properly excited by an electric line source have confirmed that the directive radiative features of these antennas can be described by the radiation of a single dominant leaky AM of the waveguide. The decomposition of the aperture field into its constituent parts was also used to describe the radiated field as the sum of a dominant and a higher order leaky-wave contribution, thus obtaining an almost perfect representation of the total far field emitted by the lattice waveguide. Once the nature of the leaky-wave radiation of these EBG structures has been explored, realistic radiators have been easily designed by truncating the lattice waveguide in order to obtain the desired leaky-wave radiation efficiency. Very good agreements have been obtained between the theoretical results based on leaky-wave radiation in conjunction with physical-optics approach and different kinds of *ad hoc* and full-wave commercial simulators.

The 2-D investigation described here is applicable to a more general class of EBG lattice structures consisting of dielectric cylinders in free space with unit cells presenting higher symmetries as well as of cylindrical holes drilled in a dielectric host. All these structures can be implemented in the design of realistic 3-D dielectric antennas at microwaves and mm-waves, where the cylinders are sandwiched between the top and bottom metal plates to mimic the 2-D environment [21].

REFERENCES

[1] D. Sievenpiper, M. Sickmiller, and E. Yablonovitch, "3D wire mesh photonic crystals," *Phys. Rev. Lett.*, vol. 76, no. 14, p. 2480, 1996.

[2] S. Enoch, G. Tayeb, P. Sabouroux, N. Guérin, and P. Vincent, "A metamaterial for directive emission," *Phys. Rev. Lett.*, vol. 89, no. 21, 2002, Art. no. 213902.

[3] P. A. Belov *et al.*, "Strong spatial dispersion in wire media in the very large wavelength limit," *Phys. Rev. B, Condens. Matter*, vol. 67, no. 11, Mar. 2003, Art. no. 113103.

[4] S. Enoch, G. Tayeb, and D. Maystre, "Dispersion diagrams of Bloch modes applied to the design of directive sources," *Prog. Electromagn. Res.*, vol. 41, pp. 61–81, 2003.

[5] S. Enoch, G. Tayeb, and B. Gralak, "The richness of the dispersion relation of electromagnetic bandgap materials," *IEEE Trans. Antennas Propag.*, vol. 51, no. 10, pp. 2659–2666, Oct. 2003.

[6] F. Yang and Y. Rahmat-Samii, *Electromagnetic Band Gap Structures in Antenna Engineering*. Cambridge, U.K.: Cambridge Univ. Press, 2008.

[7] S. Ceccuzzi, L. Pajewski, C. Ponti, and G. Schettini, "Directive EBG antennas: A comparison between two different radiating mechanisms," *IEEE Trans. Antennas Propag.*, vol. 62, no. 10, pp. 5420–5424, Oct. 2014.

[8] Y. Ju Lee, J. Yeo, R. Mittra, and W. S. Park, "Application of electromagnetic bandgap (EBG) superstrates with controllable defects for a class of patch antennas as spatial angular filters," *IEEE Trans. Antennas Propag.*, vol. 53, no. 1, pp. 224–235, Jan. 2005.

[9] F. Frezza, L. Pajewski, E. Piuzzi, C. Ponti, and G. Schettini, "Radiation-enhancement properties of an X-band woodpile EBG and its application to a planar antenna," *Int. J. Antennas Propag.*, vol. 2014, pp. 1–15, Jan. 2014.

[10] C. Ponti, P. Baccarelli, S. Ceccuzzi, and G. Schettini, "Tapered all-dielectric EBGs with 3-D additive manufacturing for high-gain resonant-cavity antennas," *IEEE Trans. Antennas Propag.*, vol. 69, no. 5, pp. 2473–2480, May 2021.

[11] T. Hayat, M. U. Afzal, F. Ahmed, S. Zhang, K. P. Esselle, and Y. Vardaxoglou, "Low-cost ultrawideband high-gain compact resonant cavity antenna," *IEEE Antennas Wireless Propag. Lett.*, vol. 19, no. 7, pp. 1271–1275, Jul. 2020.

[12] A. A. Baba, R. M. Hashmi, K. P. Esselle, Z. Ahmad, and J. Hesselbarth, "Millimeter-wave broadband antennas with low profile dielectric covers," *IEEE Access*, vol. 7, pp. 186228–186235, 2019.

[13] T. Hayat, M. U. Afzal, A. Lalbakhsh, and K. P. Esselle, "3-D-printed phase-rectifying transparent superstrate for resonant-cavity antenna," *IEEE Antennas Wireless Propag. Lett.*, vol. 18, no. 7, pp. 1400–1404, Jul. 2019.

[14] B. Ratni, E. Bochkova, G.-P. Piau, A. de Lustrac, A. Lupu, and S. N. Burokur, "Design and engineering of metasurfaces for high-directivity antenna and sensing applications," *EPJ Appl. Metamaterials*, vol. 3, 2016, pp. 1–10, Art. no. 4.

[15] C. Valagiannopoulos, T. A. Tsiftsis, and V. Kovanis, "Metasurface-enabled interference mitigation in visible light communication architectures," *J. Opt.*, vol. 21, no. 11, Nov. 2019, Art. no. 115702.

[16] Y. Shang, W. Zhou, and C. Liao, "Metasurface-based cylindrical lenses and their antenna gain enhancement," *Int. J. Antennas Propag.*, vol. 2020, pp. 1–14, Sep. 2020.

[17] R. T. Ako, A. Upadhyay, W. Withayachumnankul, M. Bhaskaran, and S. Sriram, "Dielectrics for terahertz metasurfaces: Material selection and fabrication techniques," *Adv. Opt. Mater.*, vol. 8, no. 3, Feb. 2020, Art. no. 1900750.

[18] S. Ceccuzzi, P. Baccarelli, C. Ponti, and G. Schettini, "Effect of source position on directive radiation in EBG structures with epsilon-near-zero behavior," *IEEE Antennas Wireless Propag. Lett.*, vol. 18, no. 6, pp. 1253–1257, Jun. 2019.

[19] S. Yarga, K. Sertel, and J. L. Volakis, "A directive resonator antenna using degenerate band edge crystals," *IEEE Trans. Antennas Propag.*, vol. 57, no. 3, pp. 799–803, Mar. 2009.

[20] S. Yarga, K. Sertel, and J. L. Volakis, "Degenerate band edge crystals for directive antennas," *IEEE Trans. Antennas Propag.*, vol. 56, no. 1, pp. 119–126, Jan. 2008.

[21] S. Ceccuzzi, C. Ponti, and G. Schettini, "Directive EBG antennas based on lattice modes," *IEEE Trans. Antennas Propag.*, vol. 65, no. 4, pp. 1691–1699, Apr. 2017.

[22] T. Tamir and A. A. Oliner, "Guided complex waves. Part 1: Fields at an interface," *Proc. Inst. Electr. Eng.*, vol. 110, no. 2, pp. 310–324, 1963.

[23] T. Tamir and A. A. Oliner, "Guided complex waves. Part 2: Relation to radiation patterns," *Proc. Inst. Electr. Eng.*, vol. 110, no. 2, pp. 325–334, 1963.

[24] D. R. Jackson and A. A. Oliner, "Leaky-wave antennas," in *Modern Antenna Handbook*, C. A. Balanis, Ed. Hoboken, NJ, USA: Wiley, 2008, ch. 7, pp. 325–367.

[25] C. Caloz, D. Jackson, and T. Itoh, "Leaky-wave antennas," in *Frontiers in Antennas: Next Generation Design & Engineering*, F. Gross, Ed. New York, NY, USA: McGraw-Hill, 2011, ch. 9.

[26] F. Capolino, D. R. Jackson, and D. R. Wilton, "Fundamental properties of the field at the interface between air and a periodic artificial material excited by a line source," *IEEE Trans. Antennas Propag.*, vol. 53, no. 1, pp. 91–99, Jan. 2005.

[27] G. Lovat, P. Burghignoli, F. Capolino, D. R. Jackson, and D. R. Wilton, "Analysis of directive radiation from a line source in a metamaterial slab with low permittivity," *IEEE Trans. Antennas Propag.*, vol. 54, no. 3, pp. 1017–1030, Mar. 2006.

[28] P. Burghignoli, G. Lovat, F. Capolino, D. R. Jackson, and D. R. Wilton, "Directive leaky-wave radiation from a dipole source in a wire-medium slab," *IEEE Trans. Antennas Propag.*, vol. 56, no. 5, pp. 1329–1339, May 2008.

[29] P. Burghignoli, G. Lovat, F. Capolino, D. R. Jackson, and D. R. Wilton, "Modal propagation and excitation on a wire-medium slab," *IEEE Trans. Microw. Theory Techn.*, vol. 56, no. 5, pp. 1112–1124, May 2008.

[30] G. Lovat, "Near-field shielding effectiveness of 1-D periodic planar screens with 2-D near-field sources," *IEEE Trans. Electromagn. Compat.*, vol. 51, no. 3, pp. 708–719, Aug. 2009.

[31] A. Della Villa, V. Galdi, F. Capolino, V. Pierro, S. Enoch, and G. Tayeb, "A comparative study of representative categories of EBG dielectric quasi-crystals," *IEEE Antennas Wireless Propag. Lett.*, vol. 5, pp. 331–334, 2006.

[32] A. Micco *et al.*, "Directive emission from defect-free dodecagonal photonic quasicrystals: A leaky wave characterization," *Phys. Rev. B, Condens. Matter*, vol. 79, no. 7, Feb. 2009, Art. no. 075110.

[33] G. Valerio, A. Galli, D. R. Wilton, and D. R. Jackson, "An enhanced integral-equation formulation for accurate analysis of frequency-selective structures," *Int. J. Microw. Wireless Technol.*, vol. 4, no. 3, pp. 365–372, Jun. 2012.
[34] H. Zhang, H. Zhu, L. Qian, and D. Fan, "Analysis of leaky modes of photonic crystal slabs with deeply patterned lattice," *J. Opt. A, Pure Appl. Opt.*, vol. 8, no. 5, p. 483, 2006.
[35] L. Ondič, O. Babchenko, M. Varga, A. Kromka, J. Čtyroký, and I. Pelant, "Diamond photonic crystal slab: Leaky modes and modified photoluminescence emission of surface-deposited quantum dots," *Sci. Rep.*, vol. 2, no. 1, pp. 1–6, Dec. 2012.
[36] L. Tognolatti, P. Baccarelli, V. Jandieri, S. Ceccuzzi, C. Ponti, and G. Schettini, "Directive leaky-wave radiation from a line source in 2-D EBG array of scatterers," in *Proc. URSI GASS*, 2020, pp. 1–4.
[37] V. Jandieri, P. Baccarelli, G. Valerio, K. Yasumoto, and G. Schettini, "Modal propagation in periodic chains of circular rods: Real and complex solutions," *IEEE Photon. Technol. Lett.*, vol. 32, no. 17, pp. 1053–1056, Sep. 1, 2020.
[38] P. Baccarelli, P. Burghignoli, F. Frezza, A. Galli, G. Lovat, and D. R. Jackson, "Approximate analytical evaluation of the continuous spectrum in a substrate-superstrate dielectric waveguide," *IEEE Trans. Microw. Theory Techn.*, vol. 50, no. 12, pp. 2690–2701, Dec. 2002.
[39] G. Valerio, P. Baccarelli, P. Burghignoli, A. Galli, R. Rodríguez-Berral, and F. Mesa, "Analysis of periodic shielded microstrip lines excited by nonperiodic sources through the array scanning method," *Radio Sci.*, vol. 43, no. 1, pp. 1–15, 2008.
[40] R. Rodriguez-Berral, F. Mesa, P. Baccarelli, and P. Burghignoli, "Excitation of a periodic microstrip line by an aperiodic delta-gap source," *IEEE Antennas Wireless Propag. Lett.*, vol. 8, pp. 641–644, 2009.
[41] D. Prather, A. Sharkawy, S. Shi, J. Murakowski, and G. Schneider, *Photonic Crystals, Theory, Applications and Fabrication* (Wiley Series in Pure and Applied Optics). Hoboken, NJ, USA: Wiley, 2009.
[42] V. Jandieri, P. Baccarelli, G. Valerio, and G. Schettini, "1-D periodic lattice sums for complex and leaky waves in 2-D structures using higher order Ewald formulation," *IEEE Trans. Antennas Propag.*, vol. 67, no. 4, pp. 2364–2378, Apr. 2019.
[43] V. Jandieri, K. Yasumoto, and H. Toyama, "Radiation from a line source placed in two-dimensional photonic crystals," *Int. J. Infr. Millim. Waves*, vol. 28, no. 12, pp. 1161–1173, Nov. 2007.
[44] S. Ceccuzzi, V. Jandieri, P. Baccarelli, C. Ponti, and G. Schettini, "On beam shaping of the field radiated by a line source coupled to finite or infinite photonic crystals," *J. Opt. Soc. Amer. A, Opt. Image Sci.*, vol. 33, no. 4, pp. 764–770, Apr. 2016.
[45] (2020). *CST, Computer Simulation Technology GmbH*. [Online]. Available: https://www.cst.com
[46] P. Baccarelli, S. Paulotto, D. R. Jackson, and A. A. Oliner, "A new Brillouin dispersion diagram for 1-D periodic printed structures," *IEEE Trans. Microw. Theory Techn.*, vol. 55, no. 7, pp. 1484–1495, Jul. 2007.
[47] K. Yasumoto and H. Jia, "Modeling of photonic crystals by multilayered periodic arrays of circular cylinders," in *Electromagnetic Theory and Applications for Photonic Crystals*, K. Yasumoto, Ed. Boca Raton, FL, USA: Taylor & Francis, 2010, ch. 3.
[48] P. Lampariello, F. Frezza, and A. A. Oliner, "The transition region between bound-wave and leaky-wave ranges for a partially dielectric-loaded open guiding structure," *IEEE Trans. Microw. Theory Techn.*, vol. 38, no. 12, pp. 1831–1836, Dec. 1990.
[49] A. Oliner, "Equivalent circuits: How to obtain them and use them," in *Proc. Workshop WSC, Int. Microw. Symp.*, 2000, pp. 11–16.
[50] G. Valerio, P. Burghignoli, P. Baccarelli, and A. Galli, "Input impedance of nonperiodic sources exciting 1-D periodic shielded microstrip structures," *IEEE Trans. Microw. Theory Techn.*, vol. 58, no. 7, pp. 1796–1806, Jul. 2010.
[51] P. Burghignoli, G. Lovat, and D. R. Jackson, "Analysis and optimization of leaky-wave radiation at broadside from a class of 1-D periodic structures," *IEEE Trans. Antennas Propag.*, vol. 54, no. 9, pp. 2593–2604, Sep. 2006.
[52] P. Burghignoli, P. Baccarelli, F. Frezza, A. Galli, P. Lampariello, and A. A. Oliner, "Low-frequency dispersion features of a new complex mode for a periodic strip grating on a grounded dielectric slab," *IEEE Trans. Microw. Theory Techn.*, vol. 49, no. 12, pp. 2197–2205, 2001.
[53] K. Yasumoto, H. Toyama, and T. Kushta, "Accurate analysis of two-dimensional electromagnetic scattering from multilayered periodic arrays of circular cylinders using lattice sums technique," *IEEE Trans. Antennas Propag.*, vol. 52, no. 10, pp. 2603–2611, Oct. 2004.
[54] V. Jandieri, K. Yasumoto, and B. Gupta, "Directivity of radiation from a localized source coupled to electromagnetic crystals," *J. Infr., Millim., Terahertz Waves*, vol. 30, no. 10, pp. 1102–1112, Oct. 2009.
[55] C. M. Bender and S. A. Orszag, *Advanced Mathematical Methods for Scientists and Engineers I: Asymptotic Methods and Perturbation Theory*. Cham, Switzerland: Springer, 2013.
[56] P. Baccarelli *et al.*, "Effects of leaky-wave propagation in metamaterial grounded slabs excited by a dipole source," *IEEE Trans. Microw. Theory Techn.*, vol. 53, no. 1, pp. 32–44, Jan. 2005.
[57] M. Lorente-Crespo and C. Mateo-Segura, "Highly directive Fabry–Pérot leaky-wave nanoantennas based on optical partially reflective surfaces," *Appl. Phys. Lett.*, vol. 106, no. 18, May 2015, Art. no. 183104.
[58] J. Krupka, P. Kaminski, and L. Jensen, "High Q-factor millimeter-wave silicon resonators," *IEEE Trans. Microw. Theory Techn.*, vol. 64, no. 12, pp. 4149–4154, Dec. 2016.
[59] D. R. Jackson, A. A. Oliner, and A. Ip, "Leaky-wave propagation and radiation for a narrow-beam multiple-layer dielectric structure," *IEEE Trans. Antennas Propag.*, vol. 41, no. 3, pp. 344–348, Mar. 1993.

Paolo Baccarelli (Member, IEEE) received the Laurea degree in electronic engineering and the Ph.D. degree in applied electromagnetics from "La Sapienza" University of Rome, Rome, Italy, in 1996 and 2000, respectively.

In 1996, he joined the Department of Electronic Engineering, "La Sapienza" University of Rome, where he has been an Assistant Professor since November 2010. From April 1999 to October 1999, he was a Visiting Researcher with the University of Houston, Houston, TX, USA. In 2017, he joined the Department of Engineering, Roma Tre University, Rome, where he has been an Associate Professor since 2017. In 2017, he received the National Scientific Qualification for the role of Full Professor of Electromagnetic Fields in Italian Universities. He has coauthored about 230 articles in international journals, conference proceedings, and book chapters. His research interests include analysis and design of planar antennas and arrays, leakage phenomena in uniform and periodic structures, numerical methods for integral equations and periodic structures, and propagation and radiation in anisotropic media, metamaterials, graphene, and electromagnetic bandgap structures.

Dr. Baccarelli has been a member of the TPCs of several international conferences. He was a recipient of the "Giorgio Barzilai" Laurea Prize (for the term 1994–1995) presented by the former IEEE Central and South Italy Section. He is currently an Associate Editor of the *Electronics* (MPDI), the *Magnetism* (MPDI), and the *International Journal of Antennas and Propagation* (Hindawi). He was the Secretary of the 2009-European Microwave Week (EuMW 2009).

Ludovica Tognolatti (Graduate Student Member, IEEE) was born in Rome, Italy, in April 1994. She received the B.S. and M.S. degrees *(cum laude)* in electronic engineering from Roma Tre University, Rome, in 2017 and 2019, respectively, where she is currently pursuing the Ph.D. degree with the Department of Engineering, Section of Applied Electronics.

Her current research interests include periodic structures, numerical methods, leaky-wave antennas, and electromagnetic scattering.

Vakhtang Jandieri (Senior Member, IEEE) received the Doctor of Engineering degree in computer science and communication engineering from Kyushu University, Fukuoka, Japan, in 2006.

From 2007 to 2010, he was with Kumamoto University, Kumamoto, Japan, as Post-Doctoral Japanese Society for Promotion of Science (JSPS) Fellow. He was a Visiting Professor with the School of Electronics Engineering and Computer Science, Kyungpook National University, Daegu, Republic of Korea, from 2010 to 2013, the Nanotechnology Centre, Technical University of Ostrava, Ostrava, Czech Republic, in 2015, and the Department of Engineering, Roma Tre University, Roma, Italy, in 2015. He is currently with the Department of General and Theoretical Electrical Engineering (ATE), Faculty of Engineering, University of Duisburg–Essen, Duisburg, Germany, and the Center for Nanointegration Duisburg–Essen (CENIDE), Duisburg. His research interests are in electromagnetic wave theory, and analytical and numerical techniques on microwave and optical photonic crystal devices.

Dr. Jandieri is also a Senior Member of The Optical Society (OSA). He was a recipient of the Paper Prize from the Institute of Electrical Engineers of Japan (IEEJ) in 2004; the URSI Young Scientist Award in 2010; two Fulbright Awards at the University of Illinois at Urbana–Champaign, USA, for the term 2015–2016 and the Pennsylvania State University, USA, in 2021; and the Alexander von Humboldt Award at the University of Duisburg–Essen, for the term 2016–2018.

Silvio Ceccuzzi was born in Rome, Italy, in 1983. He received the Laurea di Primo Livello and Laurea Specialistica degrees *(cum laude)* in electronic engineering and the Ph.D. degree in applied electronics from Roma Tre University, Rome, in 2005, 2008, and 2015, respectively.

After an internship at Telespazio, Rome, and Thales Alenia Space, Rome, in 2009, he started a three-year scholarship on high-power RF systems across European labs. In 2013, he joined the Italian Energy and Environment Agency, Frascati, Italy, as a Researcher, where he became responsible for the ion-cyclotron heating system of the Divertor Tokamak Test facility in 2021. Since 2016, he has been a Visiting Researcher at Roma Tre University. He has authored or coauthored more than 100 works on technical reports, journals, and conference proceedings. His current research interests include electromagnetic bandgap (EBG), microwave components, and nuclear fusion.

Dr. Ceccuzzi received the 2015 IEEE MTT-S Award of the Chapter Central and Southern Italy and the "Sannino" Award of the Italian meeting RiNEm 2012.

Cristina Ponti (Member, IEEE) received the Laurea and Laurea Magistralis degrees *(cum laude)* in electronic engineering from the "Sapienza" University of Rome, Rome, Italy, in 2004 and 2006, respectively, and the Ph.D. degree from Roma Tre University, Rome, in March 2010.

In 2006, she joined the Applied Electronics Department, Roma Tre University, Rome, where she attended the Doctoral School in Biomedical Engineering, Electromagnetism, and Telecommunications from November 2006 to October 2009. From February to December 2010, she was an Assistant Researcher. Since December 2010, she has been a Researcher in electromagnetic fields. Her main research interests are in electromagnetic analysis, scattering problems, buried-objects detection, ground-penetrating radar, through-the-wall radar, numerical methods, electromagnetics-bandgap materials, antennas, and microwave components for high-power applications.

Dr. Ponti is a member of the IEEE Antennas and Propagation, Geoscience and Remote Sensing and Women in Engineering Societies, the National Interuniversity Consortium for Telecommunications (CNIT), and the Italian Society of Electromagnetics (SIEm). She was a Co-Convener of conference sessions at URSI EMTS 2016, URSI EMTS 2019, and URSI GASS 2021. She is an Associate Editor of *IET Microwaves, Antennas and Propagation*.

Giuseppe Schettini (Senior Member, IEEE) received the Laurea degree *(cum laude)* in electronic engineering, the Ph.D. degree in applied electromagnetics, and the Laurea degree *(cum laude)* in physics from the "La Sapienza" University of Rome, Rome, Italy, in 1986, 1991, and 1995, respectively.

Upon his graduation in electronic engineering, he joined the Italian Energy and Environment Agency (ENEA), Frascati, Italy, where he was initially involved with free electron generators of millimeter waves and then on microwave components and antennas for heating of thermonuclear plasmas. In 1992, he joined "La Sapienza" University as Researcher of electromagnetics. In 1998, he joined the Department of Engineering, Section of Applied Electronics, Roma Tre University, Rome, where he was an Associate Professor from 1998 to 2005 and he has been a Full Professor of electromagnetic fields since 2005. From 2013 to 2017, he has been the Deputy Director for Research of the Department of Engineering. He is currently the Rector's delegate for North America technology transfer. His scientific research is focused on structures for guiding and radiation of electromagnetic fields for microwave and millimeter-wave applications, scattering, diffractive optics, plasma heating and current drive, electromagnetic bandgap (EBG) media, and anisotropic media.

Dr. Schettini is a member of several scientific and technical societies in the framework of information technology, in particular in the field of electromagnetic systems. He is also a member of the editorial boards and technical program committees of several international journals and conferences in the field of microwaves and antennas. He is an Associate Editor of the IEEE OPEN JOURNAL OF ANTENNAS AND PROPAGATION.